Journal of Modern Researches on Electronic Defense Systems

Receive: 20 July 2025 Accept: 9 September 2025

Microwave absorbing application of B-Co doped magnetic Graphene: a first principle study

Mahdi Zarepour*[1], Hamed Asadi[2]

*Corresponding Author: mehdizare@aut.ac.ir

[1] Department of Electrical Engineering, K. N Toosi University of Technology, Tehran, Iran.
[2] Department of Electrical Engineering, Amirkabir University of Technology, Tehran, Iran

Abstract – *The application of graphene-based nanomaterials in microwave absorption has been hindered by high electrical conductivity and excessive dielectric loss, which lead to poor impedance matching. A promising strategy to address this is to achieve optimal impedance matching by utilizing ferromagnetic graphene nanocomposites with suppressed conductivity. In this study, we synthesized and investigated boron-doped and cobalt-decorated graphene (GBCo) for this purpose. Density Functional Theory (DFT) calculations were employed to model the impedance parameters and predict reflection loss. The GBCo nanocomposite exhibited enhanced dielectric properties, which are attributed to interfacial charge transfer, resulting in outstanding microwave absorption performance across a broad frequency range. Among the synthesized variants (GCo22, GCo33, and GBCo33), the GBCo22 nanocomposite demonstrated superior performance, with a maximum reflection loss (RL) of -42.02 dB. This exceptional absorption is due to favorable impedance matching and an optimized balance between dielectric and magnetic loss mechanisms. The results indicate that the proposed GBCo22 structure achieves effective absorption (RL < -10 dB) across the entire 2-18 GHz frequency band.*

Keywords: *Graphene, Microwave Absorbing Material, Ferromagnetic, Magnetization, Nano Composite, Density Functional Theory (DFT).*

1. Introduction

The rapid development and proliferation of electronics and communication devices have led to growing concerns about electromagnetic radiation pollution. This pollution poses significant risks to human health and can disrupt the operation of sensitive electronic equipment. One solution to mitigate this problem is the use of electromagnetic interference (EMI) shielding and microwave-absorbing materials, which function by absorbing electromagnetic waves and converting them into heat or attenuating them at the interface [1-5]. Ideal microwave absorbing materials should be lightweight, possess strong absorption capabilities, offer broad bandwidth, and have a small thickness [6]. Absorbers can be classified based on different parameters, but considering the general absorption mechanism, they are primarily divided into two categories: (1) dielectric loss materials, such as dielectric ceramics [7-10] and carbon-based materials [11-14], and (2) magnetic loss material, including ferrites [15-17], magnetic metals and their alloys [18-25]. Ceramics offer several tunable properties, enabling desired characteristics such as thermal stability, environmental resistance, selectable mechanical properties for structural absorbers, and excellent dielectric loss at middle and low frequencies. However, their permittivity often decreases at high frequencies, necessitating heavy loading or increased thickness to achieve practical microwave absorbing performance [10]. Single-component magnetic or dielectric materials often fail to meet all the requirements of an ideal absorber. They typically absorb only the magnetic or electric component of electromagnetic waves, respectively, which can result in poor impedance matching and consequently weak electromagnetic wave absorption performance. Therefore, material compositing has emerged as a highly successful strategy for improving absorber properties, attracting significant research attention. A critical concept in electromagnetic wave absorption is the impedance matching between the absorber and free space. Superior impedance matching leads to lower reflection loss (RL). Ideally, all incident electromagnetic waves would enter the absorber without reflection, a condition achieved when Zin = Z0 (i.e., when the normalized characteristic impedance

Z = Zin / Z0 is equal to 1). However, since the electromagnetic parameters of a material constantly change with frequency, achieving this condition over a wide bandwidth is challenging. Different materials may only meet this condition within a narrow frequency range. One effective method to broaden this range is through the fabrication of composite materials with tailored impurities. Graphene and its derivatives have attracted extensive interest due to their exceptional electromagnetic, optical, and physical properties, alongside numerous potential applications. Its large specific surface area, low density, and high chemical stability also make it an ideal coating material. It has been reported that interfacial electronic interactions between metal atoms and graphene derivatives can enhance charge carrier density, facilitate charge transfer, and alter the magnetic and electronic properties of graphene, leading to novel electrical and magnetic behaviors in metal-graphene heterostructures.

Results from numerous studies indicate that the edges of graphene play a crucial role in determining its electromagnetic properties [26-32]. Several studies on graphene-based materials have demonstrated the importance of edge states arising from non-bonding edge electrons, impurities (such as dopants, defects, and adsorbates), and a high surface-to-volume ratio (aspect ratio). These materials have been reported to exhibit unusual magnetic properties, including spin-glass behavior and magnetic switching phenomena [33-35]. Bilayer Graphene is predicted to be ferromagnetic [36], and hydrogenated graphene-based materials have shown spontaneous magnetism [37]. The magnetic properties of graphene derivatives, reviewed by Enoki et al., conclude that edge states as well as adsorbed or intercalated species significantly affect magnetic behavior [38], [39]. Laminated magnetic graphene shows substantial changes in electromagnetic properties compared to pure graphene [40]. Results indicate that a reflection loss below -10 dB was obtained at 10.4-13.2 GHz, confirming graphene's potential as a highly desirable electromagnetic wave absorber. Quan et al. showed that nitrogen-doped graphene can achieve a maximum absorption of -11.3 dB at 12.7 GHz and an absorption bandwidth of 12.2–14.3 GHz (RL < -10 dB) at a thickness of 3 mm [41]. Wang and co-workers indicated that reduced graphene oxide (r-GO) exhibits much better microwave absorbing ability than graphite [42]. Polyaniline (PANI), one of the most promising conducting polymers, possesses excellent physical stability, high electrical conductivity, and microwave absorption capabilities [43-45]. Composites of reduced graphene oxide with polyaniline film (2 mm thickness) exhibit a high reflection loss of -41.4 dB at 13.8 GHz, attributed to unique structural characteristics and charge transfer between RGO and PANI [46]. Yao et al. demonstrated that Co nanospheres supported on nitrogen-doped graphene (with a thickness of 1.3 mm) show a maximum reflection loss (RL) of -24.3 dB at 17.7 GHz. The effective absorption bandwidth (RL < -10 dB) ranges from 3.6 to 18 GHz when the absorber nanocomposite thickness is between 1.2 and 4.0 mm [46].

The performance of microwave absorbers is fundamentally governed by their complex permittivity and permeability, which determine the impedance matching and attenuation capabilities. While theoretical modeling provides profound insights, experimental validation of these electromagnetic parameters is crucial for practical applications. Recent precise experimental investigations have highlighted the significance of accurately characterizing the complex permittivity in advanced materials. For instance, Hossein-Babaei and Chegini conducted a meticulous study on the complex permittivity of the conducting polymer PEDOT:PSS, demonstrating how its dielectric properties are critically influenced by material composition and frequency [47]. Their work underscores the importance of empirical measurement and control of permittivity for optimizing microwave absorption. In alignment with this approach, our first-principles study aims to theoretically predict and analyze the complex permittivity and impedance matching in B-Co doped graphene nanocomposites. By leveraging Density Functional Theory, we seek to provide a foundational understanding of the charge transfer and polarization mechanisms that dictate the dielectric response, thereby bridging the gap between theoretical predictions and the empirical trends observed in experimental studies like those on PEDOT:PSS.

This work provides a new strategy for constructing novel lightweight magnetic/dielectric nanocomposites based on B-doped and Co-decorated graphene for high-efficiency electromagnetic wave absorption. To the best of our knowledge, this is one of the first articles to systematically describe the microwave response of such nanocomposites using a DFT-based approach.

2. Simulations and Calculations

2.1. Simulation method

All calculations were performed using Density Functional Theory (DFT) as implemented in the Quantum ESPRESSO (QE) code. Electron exchange and correlation effects were described using the generalized gradient approximation (GGA) with the Perdew-Burke-Ernzerhof (PBE) functional. The electron-ionic core interaction was represented using Optimized Norm-Conserving Vanderbilt Pseudopotentials (ONCVPSP) in UPF format, which offer higher accuracy than typical ultrasoft pseudopotentials [48]. The plane-wave basis set for the electron wavefunction was expanded with an energy cutoff of 45 Ry to ensure accurate results. Brillouin

zone integration was performed using the Monkhorst-Pack scheme with an 8×8×1 k-point mesh. The initial C-C bond length was set to 1.42 Å. Molecular dynamics (MD) simulations were performed to extract basis sets in the temperature-equivalent frequency range of 1-18 GHz. The dopant and adsorption energies were calculated using the following equation:

$$E_b = E_t - (E_s + E_a) \quad (1)$$

Where E_b, E_t, E_s and E_a are the binding energy, total energy of the system, total energy of the substrate (graphene), and energy of the adsorbate atom (Co) in isolation, respectively. The XGαα/Y configuration was used to investigate the effect of supercell size and impurity density on the mechanical, electrical, and magnetic characteristics of graphene, where X= {{}, B}, Y= {{}, Co} and α= {2, 3} which indicates 2×2 and 3×3 supercells consisting of 8 and 18 atoms, respectively. As shown in Figure 1, this nomenclature yields eight possible configurations: {G22, GB22, GCo22, GBCo22, G33, GB33, GCo33, GBCo33}. First, molecular dynamics (MD) simulations were run by setting the temperature corresponding to the frequency range (1-18 GHz), followed by structural relaxation calculations to obtain optimized energies, bond lengths, and geometries. Subsequently, self-consistent field (SCF), non-self-consistent field (NSCF), band structure, and density of states (DOS) calculations were performed to determine the basis sets, magnetization, Fermi energy, asymmetric basis sets, electron motion in reciprocal space, and electron distribution across energy levels. Finally, NMR and dielectric constant (epsilon) calculations were conducted to compute the frequency-dependent impedance parameters, specifically permeability and permittivity. In the final stage, the adsorption of a gaseous Co atom onto Gαα and GBαα was simulated. Boron and Cobalt were selected because B-doping creates a strong positive anchoring point for transition metal adsorption (as found in our previous study [49]), and Co chemisorption induces magnetism in graphene [50]. For this purpose, the Co was initially placed 3 Å above the GXαα.

2.1 Theoretical method

The Quantum ESPRESSO package allows for the direct calculation of the complex dielectric function and the magnetic susceptibility, from which the complex permeability at different frequencies can be derived. The relative permeability is calculated from:

$$\mu_r = 1 + \chi_m \quad (2)$$

The relative permeability consists of real and imaginary parts:

$$\mu_r = \mu' - i\mu'' \quad (3)$$

$$|\mu_r| = \sqrt{\mu'^2 + \mu''^2} \quad (4)$$

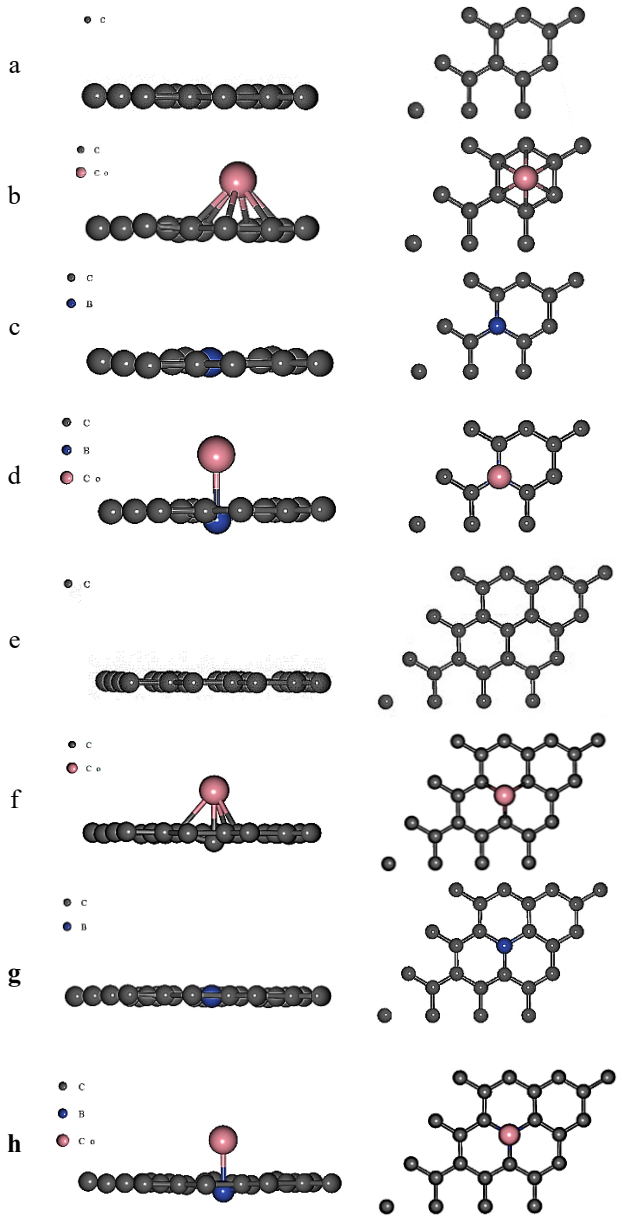

Figure.1: Morphological results of calculations, G22 (a), GCo22 (b), GB22 (c), GBCo22 (d), G33 (e), GCo33 (f), GB33 (g) and GBCo33 (h)

The imaginary part of the permeability (μ"), which represents losses due to magnetic moment relaxation, is related to the real part (μ') through the following equation:

$$\mu'' = 2\pi f \mu_0 \mu'^2 d^2 \sigma_{ac} \quad (5)$$

Where f, d and, σ_{ac} represent the frequency, thickness, and alternating conductivity of the composite, respectively. Alternating conductivity is linearly related to the frequency and the imaginary part of the permittivity:

$$\sigma_{ac} = 2\pi\varepsilon_0 f \varepsilon'' \quad (6)$$

Substituting Equation (6) into Equation (5), and then substituting the result into the definition of $|\mu_r|$, we obtain:

$$\mu'' = 4\pi^2 \varepsilon_0 f^2 \mu_0 \mu'^2 d^2 \varepsilon'' \quad (7)$$

$$\mu^{"} = \alpha\mu'^{2} \quad (8)$$

$$\alpha = 4\pi^2\varepsilon_0 f^2 \mu_0 d^2 \varepsilon^{"} \quad (9)$$

$$\chi_m = \mu'\sqrt{1+\alpha\,\mu'^{2}} - 1 \quad (10)$$

For electromagnetic shielding, the reflection loss (RL) is a function of impedance and is expressed by Equation (11), where Z_{in} is the input impedance for the surfaces of the shielding material and Z_0 is the intrinsic impedance of the space (377Ω). Z_{in} is expressed by the Equation (12):

$$RL(dB) = 20log\left[\frac{Z_{in}-Z_o}{Z_{in}+Z_o}\right] \quad (11)$$

$$Z_{in} = \sqrt{\frac{\mu_r}{\varepsilon_r}}tanh\,[j\left(\frac{2\pi\omega d}{c}\right)\sqrt{\mu_r.\,\varepsilon_r} \quad (12)$$

An excellent approximation of the magnetic susceptibility can be obtained from the output of NMR calculations, specifically the chi_bare (pGv-HH) parameter. All calculations were performed for a sample thickness of 1 mm.

3. Results

3.1. Mechanical results

Optimal bond lengths and energies extracted from MD and structural optimization calculations are listed in Table 1. The results demonstrate that the Co adsorption energy increased significantly from -0.910 eV to -1.662 eV for GBCo22 and from -0.892 eV to -1.562 eV for GBCo33. These values are higher (more negative) than the result of -1.13 eV reported by Cao et al. [49], indicating that the GBCoαα structures are more stable than GCoαα under environmental conditions. For pristine Gαα, the optimal C-C bond length was 1.418 Å. Replacing a central C atom with a B atom resulted in B-C bond lengths of 1.452 Å and 1.465 Å for GB22 and GB33, respectively. The minimum distance between cobalt and the graphene plane was 1.651 Å for GBCo22, which is reasonable given its highly negative adsorption energy and is consistent with previous works [49], [50].

2.1 Electromagnetic results

As shown in Equation (13), magnetization (M) is linearly proportional to the difference between spin-up (N^+) and spin-down (N^-) electrons [51]. For GCoαα structures, the formation of multiple bonds between Co and graphene reduces the number of free electrons, consequently decreasing the magnetization M. Conversely, in GBCoαα structures, the single strong bond between Co and the positively polarized B anchoring point increases the number of free electrons, enhancing magnetization. Furthermore, magnetization breaks symmetry and induces band splitting. From the minimization condition for the total energy, the equilibrium condition for spin splitting is given by Equation (14) [51]. Therefore, strong magnetization leads to large band splitting. The extent of band splitting and the effect of magnetization on the band structure and DOS are presented in Figures 2 and 3, respectively.

$$M = (N^+ - N^-)\mu_B \quad (14)$$

$$\Delta\varepsilon = (\varepsilon^+ - \varepsilon^-) = I_s M \quad (15)$$

I_s is the effective exchange parameter in the Stoner model [52]. Lower DOS at the Fermi level generally leads to stronger ferromagnetism. According to the Stoner criterion, the susceptibility (χ), which is the system's response function, is inversely related to the DOS. If the susceptibility is small, the system's response to external perturbations (e.g., magnetic field, pressure) is weak because the magnetic moment cannot readily follow the perturbation. The occurrence of the Fermi level within a band gap or a spin-up band leads to strongly ferromagnetic behavior [51].

$$\frac{1}{\chi} = \alpha\left(\frac{1}{\mathcal{N}(\varepsilon^+)} - \frac{1}{\mathcal{N}(\varepsilon^-)}\right) + \beta \quad (15)$$

χ, $\mathcal{N}$, α and β are susceptibility, number of states and constants, respectively. As can be seen in Figures 2 and 3, Composites without Co are non-magnetic, while those containing both B and Co exhibit stronger ferromagnetism than those with Co alone.

Table 1. Results of mechanical optimization and magnetization

Composite	*Total Energy (eV)*	*Binding Energy (eV)*	*Total Magnetization (Bohr mag/cell)*	*ABS Magnetization (Bohr mag/cell)*	*Co-GR distance (Å)*
G22	-1234.428	-	0	0	-
G33	-2777.496	-	0	0	-
G22/Co	-4831.779	-0.911	1.050	1.200	1.772
G33/Co	-6446.417	-0.892	0.940	1.260	1.891
BG22	-1155.692	-1.230	0	0	-
BG33	-2698.982	-1.189	0	0	-
BG22/Co	-4828.282	-1.662	1.980	2.240	1.651
BG33/Co	-6371.436	-1.526	1.940	2.430	1.687

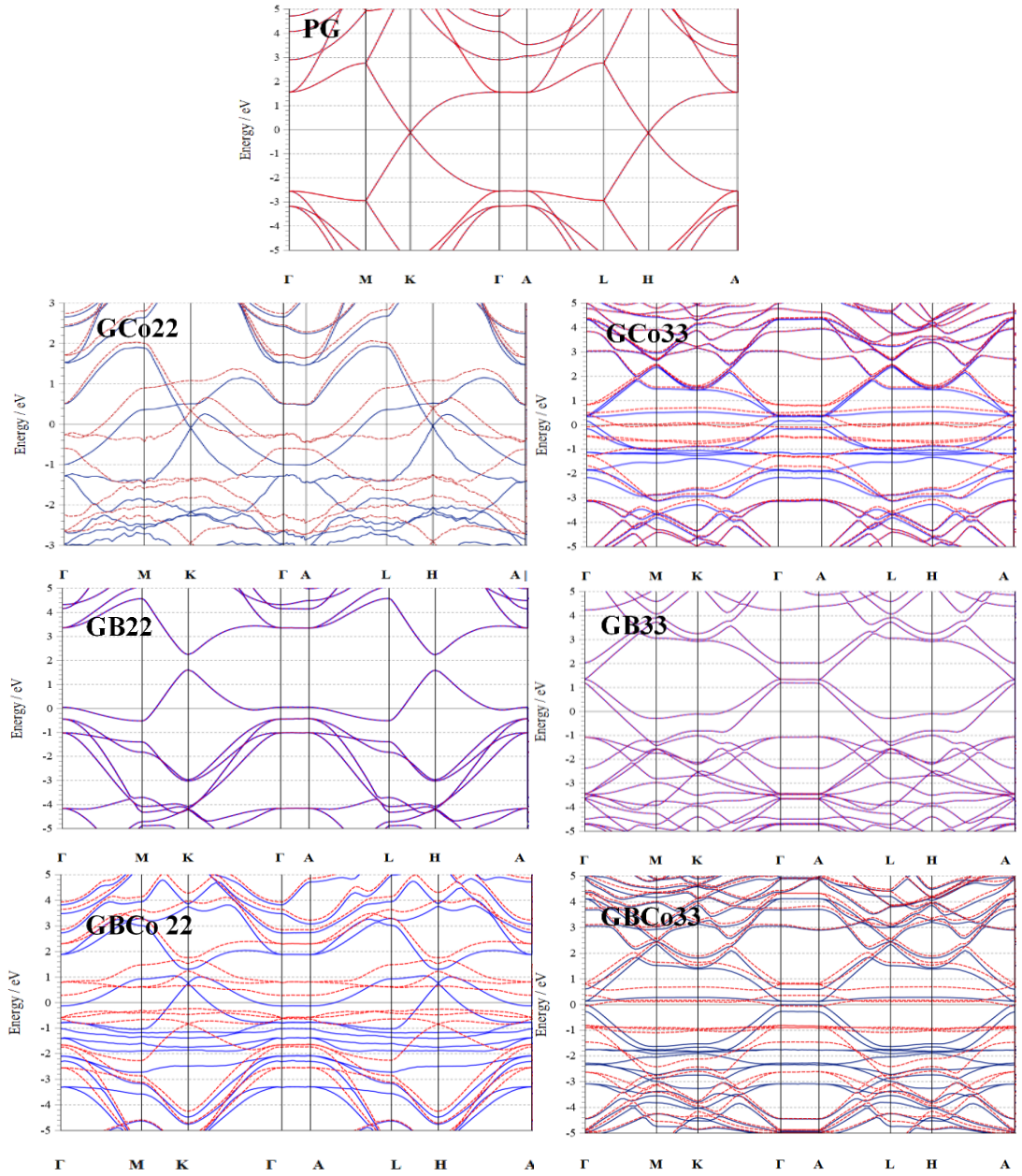

Figure 2. Band structure of the eight compositions; the spin-up channel is represented by a blue line and the spin-down channel by a red dotted line.

An efficient electromagnetic wave absorber must meet the dual requirements of strong absorption amplitude and broad absorption bandwidth. The complex permittivity ($\varepsilon_r = \varepsilon' - j\varepsilon''$) and complex permeability ($\mu_r = \mu' - j\mu''$) of the composites are shown in Figure 4. The real parts, ε' and μ', represent the ability to store electric and magnetic energy, respectively. The imaginary parts, ε" and μ", are associated with energy dissipation (dielectric and magnetic losses). As shown in Figure 4, the values of ε', ε", and μ' generally decrease with increasing frequency from 2.0 to 18.0 GHz. The imaginary permeability μ" is generally less than one and fluctuates with frequency, showing a slight increasing trend for GBCoαα in some ranges. ε' represents the polarizability of the material, comprising dipolar and electronic polarization contributions at microwave frequencies. High ε' values indicate high levels of electronic polarization and electrical conductivity, facilitated by electron transfer between Co and the graphene substrate. Resonance peaks in the ε' curve suggest relaxation processes originating from interfacial (Maxwell-Wagner) polarization. The ε' values and resonance peaks are higher for GBCoαα nanocomposites than for GCoαα. These peaks in heterogeneous systems (composed of BGαα and Co) arise from surface polarization effects due to contrasts in

conductivity and permittivity between components. A significant peak appears in the 2-4 GHz range in the μ' spectrum of the GCo22 composite and in the 6-8 GHz range for GCo33. An interesting case is observed in the μ' spectrum of GBCo22, which shows two relatively strong peaks near 7 GHz and 13 GHz. The first peak aligns with the peak position for GCo33, and the second aligns with a peak for GBCo33. Dielectric and magnetic losses are the two main factors governing reflection loss. Tuning the balance between these two loss mechanisms is crucial for enhancing microwave absorption performance. Figure 5 shows the dielectric loss tangent (tan $\delta_\varepsilon = \varepsilon''/\varepsilon'$) and magnetic loss tangent (tan $\delta_\mu = \mu''/\mu'$) for the composites. The dielectric loss in GCoαα structures is higher than in other composites, but their magnetic loss is low; consequently, loss matching is achieved only over a narrow frequency range. However, in GBCoαα composites, the dielectric and magnetic losses converge as frequency increases, enhancing absorption and improving impedance matching.

The balance between dielectric and magnetic loss in an absorber, dictated by its impedance matching properties, is key to optimizing reflection loss performance. High electrical conductivity can lead to poor impedance matching, increasing wave reflectivity. To achieve efficient absorbers, an optimal balance between impedance matching and attenuation constant must be found, requiring appropriate electromagnetic parameters[53]. The Co and B impurities added to graphene modify its properties differently: Co increases conductivity by injecting electrons from its conduction band into graphene, while B decreases conductivity due to having one less valence electron than carbon. As shown in Figure 6, B-doping reduces conductivity and improves impedance matching. In other words, the addition of p-type (B) impurities effectively reduces electrical conductivity, leading to better impedance matching with free space and thereby reducing wave reflection and enhancing absorption capacity.

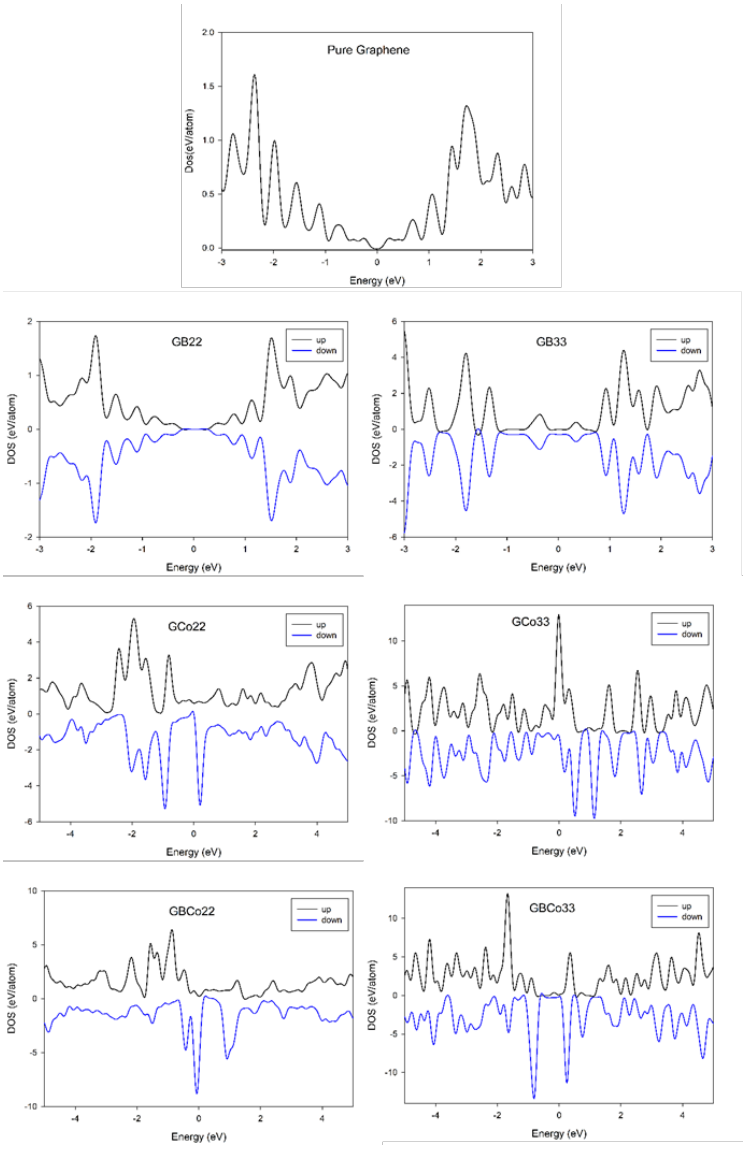

Figure 3. Density of States (DOS) of the compositions

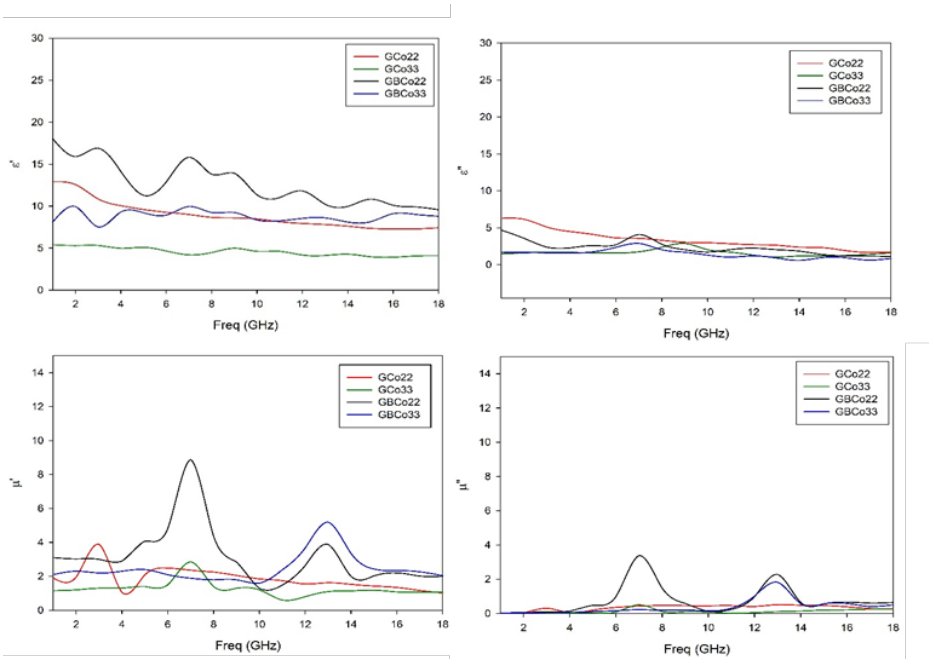

Figure 4. Magnetic and dielectric parameters of composites

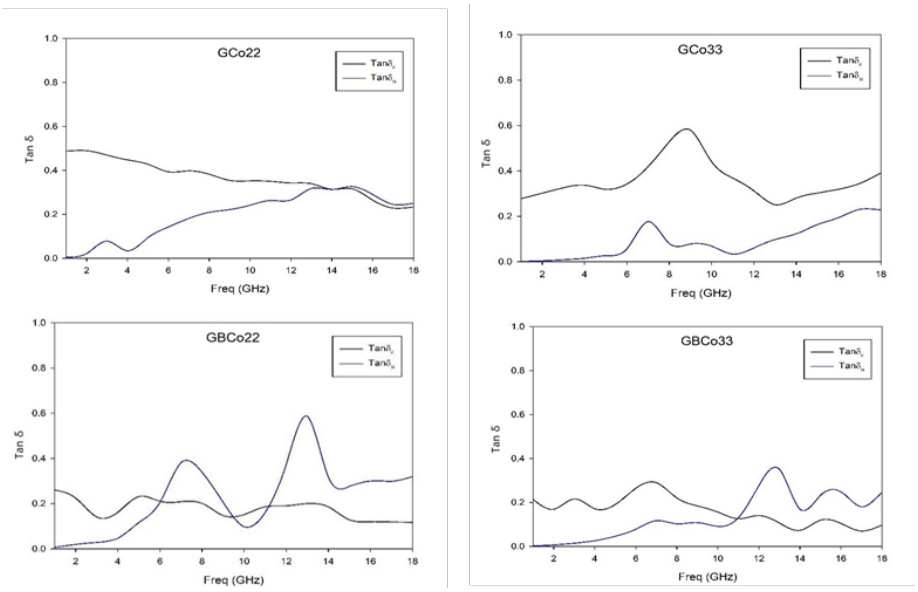

Figure 5. Magnetic and dielectric loss calculated by DFT and Theory

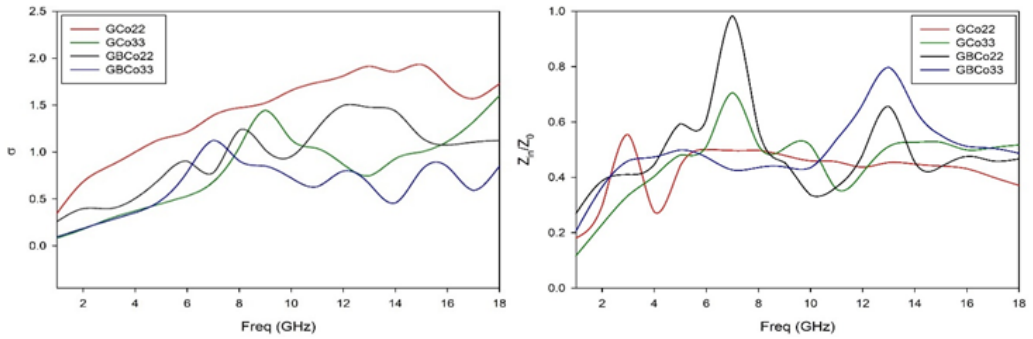

Figure 6. Impedance and ac conduction calculated by DFT and theoretical calculations

Polarization relaxation and electrical conductivity are two essential mechanisms for electromagnetic energy dissipation in nanocomposites. The maximum RL parameters are summarized in Table 2. It was found that the microwave absorption properties are strongly influenced by the adsorbate concentration and supercell size. As shown in Figure 7, compared to GCo22, GCo33, and GBCo33 nanocomposites, GBCo22 exhibits superior microwave absorption efficiency due to its excellent impedance matching and optimal balance between dielectric and magnetic losses. The GCo22 nanocomposite has the highest reflection loss (least absorption) of -10.87 dB at 3 GHz, due to its high conductivity and poor impedance matching (Z_{max} = 0.55). Its bandwidth (RL < -10 dB) is 0.6 GHz (2.6-3.2 GHz). For the GCo33 composite, impedance matching improves (Z = 0.71 at 7 GHz), resulting in a lower RL of -15.28 dB at 7 GHz and a broader -10 dB bandwidth of 2.1 GHz (6.0-8.1 GHz). GBCo22 shows the highest absorption (lowest RL) among all nanocomposites, achieved through excellent impedance matching (Z ≈ 0.98) and reduced conductivity via B-doping. Its maximum reflection loss is -42.02 dB at 7 GHz. Notably, this sample exhibits three distinct absorption peaks below -10 dB: the main peak at 7 GHz (-42.02 dB), a second peak at 13 GHz (-13.67 dB), and a third around 5 GHz. The -10 dB bandwidth for the main peak is 2.2 GHz (5.8-8.0 GHz), and for the second peak, it is 1.7 GHz (12.1-13.8 GHz). The bandwidth for RL < -20 dB (99% absorption) for the main peak is 1.8 GHz (6.1-7.9 GHz). For the GBCo33 structure, the maximum reflection loss is -18.96 dB at 13 GHz (Z=0.78), with a very broad -10 dB bandwidth of 4.7 GHz (10.9-15.6 GHz). For the GBCo33 structure, the maximum reflectance loss was -18.96 dB in the range of 10.9 to 15.6 with a bandwidth of 4.7 GHz, corresponding to an impedance matching of 0.79 at 13 GHz.

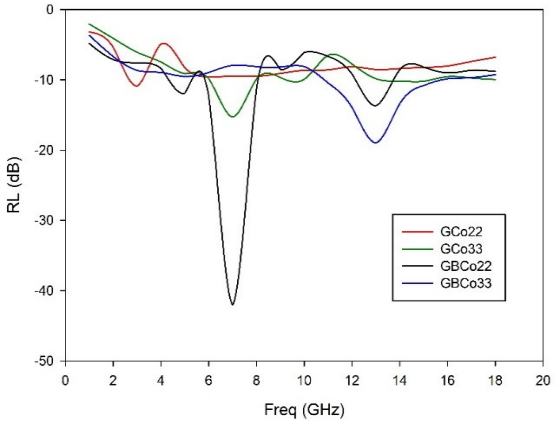

Figure 7. Reflection loss (RL) spectra calculated by DFT and theory.

Electromagnetic waves within a material can be converted into other forms of energy, such as heat. The GBCoαα nanocomposites form a large three-dimensional cross-linked network and a complex conductive lattice structure, which can generate a strong, broadband electromagnetic response [54]. Induced currents within this network can be rapidly dissipated and converted into thermal energy through ohmic losses. The surface of magnetic GBCoαα, with its strong magnetic anchoring points and excellent dielectric performance, makes it a promising candidate for electromagnetic shielding and microwave absorption applications.

Table 2. The maximum RL parameters of magnetic GXCoαα nanocomposites.

Composite	Z_{Max} (Z_{in} / Z_0)	*Frequency (Hz)*	$tan\delta_\varepsilon$	$tan\delta_\mu$	*RL (dB)*
GCo22	0.55	3	0.47	0.08	-10.87
GCo33	0.71	7	0.42	0.18	-15.28
GBCo22	0.98	7	0.21	0.38	-42.02
GBCo 33	0.78	13	0.29	0.35	-18.96

5. Conclusions

Density functional theory calculations using the Quantum ESPRESSO package with Optimized Norm-Conserving Vanderbilt Pseudopotentials (ONCVPSP), combined with theoretical modeling, were employed to investigate the mechanical and electromagnetic properties of GXYαα compositions (x= {{}, B, Co}, y= {{}, Co} and α= {2, 3}). The results emphasize that B-doping enhances the physical stability of the structures by creating a positive anchoring point. Subsequent Co decoration on B-doped graphene (GBαα) induces spin-polarized band splitting, resulting in a transition from a non-magnetic to a ferromagnetic structure. This composite is suitable for magnetic applications and electromagnetic shielding due to the induced magnetism and the high inherent thermal and electrical conductivity of graphene. An absorption level below -10 dB corresponds to a 90% attenuation of the incident wave, meeting the practical application standard for absorbers. An RL value below -20 dB indicates 99% absorption. Based on these benchmarks, the GBCo22 nanocomposite is predicted to exhibit excellent performance in electromagnetic protection applications, a direct result of its near-perfect impedance matching and optimal balance between electrical and magnetic loss characteristics.

References

[1] A. V. Kramarenko and U. Tan, "Effects of high-frequency electromagnetic fields on human EEG: a brain mapping study," *Int. J. Neurosci.*, vol. 113, no. 7, pp. 1007–1019, 2003.

[2] M. H. Al-Saleh and U. Sundararaj, "Electromagnetic interference shielding mechanisms of CNT/polymer composites," *Carbon*, vol. 47, no. 7, pp. 1738–1746, 2009.

[3] S. J. Genuis, "Fielding a current idea: exploring the public health impact of electromagnetic radiation," *Public Health*, vol. 122, no. 2, pp. 113–124, 2008.

[4] X. Sun *et al.*, "Laminated magnetic graphene with enhanced electromagnetic wave absorption properties," *J. Mater. Chem. C*, vol. 1, no. 4, pp. 765–777, 2013.

[5] D. Liu, P. Liu, Q. Yang, G. Tang, L. Zhao, and F. Zeng, "Research status and prospect of wave absorbing materials," *Mater. Rev.*, vol. 27, no. 17, pp. 74–78, 2013.

[6] F. Qin and C. Brosseau, "A review and analysis of microwave absorption in polymer composites filled with carbonaceous particles," *J. Appl. Phys.*, vol. 111, no. 6, 2012.

[7] G. Wu, Y. Cheng, Q. Xie, Z. Jia, F. Xiang, and H. Wu, "Facile synthesis of urchin-like ZnO hollow spheres with enhanced electromagnetic wave absorption properties," *Mater. Lett.*, vol. 144, pp. 157–160, 2015.

[8] S. Bi, X. Su, G. Hou, C. Liu, W.-L. Song, and M.-S. Cao, "Electrical conductivity and microwave absorption of shortened multi-walled carbon nanotube/alumina ceramic composites," *Ceram. Int.*, vol. 39, no. 5, pp. 5979–5983, 2013.

[9] Y. Qing, J. Su, Q. Wen, F. Luo, D. Zhu, and W. Zhou, "Enhanced dielectric and electromagnetic interference shielding properties of FeSiAl/Al2O3 ceramics by plasma spraying," *J. Alloys Compd.*, vol. 651, pp. 259–265, 2015.

[10] Q. Yuchang, W. Qinlong, L. Fa, Z. Wancheng, and Z. Dongmei, "Graphene nanosheets/BaTiO 3 ceramics as highly efficient electromagnetic interference shielding materials in the X-band," *J. Mater. Chem. C*, vol. 4, no. 2, pp. 371–375, 2016.

[11] H. Pan, X. Yin, J. Xue, L. Cheng, and L. Zhang, "In-situ synthesis of hierarchically porous and polycrystalline carbon nanowires with excellent microwave absorption performance," *Carbon*, vol. 107, pp. 36–45, 2016.

[12] N. Li *et al.*, "Electromagnetic interference (EMI) shielding of single-walled carbon nanotube epoxy composites," *Nano Lett.*, vol. 6, no. 6, pp. 1141–1145, 2006.

[13] Y. Qing, W. Zhou, S. Huang, Z. Huang, F. Luo, and D. Zhu, "Evolution of double magnetic resonance behavior and electromagnetic properties of flake carbonyl iron and multi-walled carbon nanotubes filled epoxy-silicone," *J. Alloys Compd.*, vol. 583, pp. 471–475, 2014.

[14] X. Su, J. Zhang, Y. Jia, Y. Liu, J. Xu, and J. Wang, "Preparation and microwave absorption property of nano onion-like carbon in the frequency range of 8.2–12.4 GHz," *J. Alloys Compd.*, vol. 695, pp. 1420–1425, 2017.

[15] H. Lv *et al.*, "Coin-like α-Fe2O3@ CoFe2O4 core–shell composites with excellent electromagnetic absorption performance," *ACS Appl. Mater. Interfaces*, vol. 7, no. 8, pp. 4744–4750, 2015.

[16] G. Tong, W. Wu, J. Guan, H. Qian, J. Yuan, and W. Li, "Synthesis and characterization of nanosized urchin-like α-Fe2O3 and Fe3O4: microwave electromagnetic and absorbing properties," *J. Alloys Compd.*, vol. 509, no. 11, pp. 4320–4326, 2011.

[17] Y. Zong *et al.*, "One-pot, template-and surfactant-free solvothermal synthesis of high-crystalline Fe3O4 nanostructures with adjustable morphologies and high magnetization," *J. Magn. Magn. Mater.*, vol. 423, pp. 321–326, 2017.

[18] J. Liu, M.-S. Cao, Q. Luo, H.-L. Shi, W.-Z. Wang, and J. Yuan, "Electromagnetic property and tunable microwave absorption of 3D nets from nickel chains at elevated temperature," *ACS Appl. Mater. Interfaces*, vol. 8, no. 34, pp. 22615–22622, 2016.

[19] X. Li, X. Guo, T. Liu, X. Zheng, and J. Bai, "Shape-controlled synthesis of Fe nanostructures and their enhanced microwave absorption properties at L-band," *Mater. Res. Bull.*, vol. 59, pp. 137–141, 2014.

[20] G. Tong, Q. Hu, W. Wu, W. Li, H. Qian, and Y. Liang, "Submicrometer-sized NiO octahedra: facile one-pot solid synthesis, formation mechanism, and chemical conversion into Ni octahedra with excellent microwave-absorbing properties," *J. Mater. Chem.*, vol. 22, no. 34, pp. 17494–17504, 2012.

[21] X. Fan, J. Guan, Z. Li, F. Mou, G. Tong, and W. Wang, "One-pot low temperature solution synthesis, magnetic and microwave electromagnetic properties of single-crystal iron submicron cubes," *J. Mater. Chem.*, vol. 20, no. 9, pp. 1676–1682, 2010.

[22] B. Zhao, W. Zhao, G. Shao, B. Fan, and R. Zhang, "Morphology-control synthesis of a core–shell structured NiCu alloy with tunable electromagnetic-wave absorption capabilities," *ACS Appl. Mater. Interfaces*, vol. 7, no. 23, pp. 12951–12960, 2015.

[23] Y. Cheng *et al.*, "Facile synthesis of FeCo alloys with excellent microwave absorption in the whole Ku-band: Effect of Fe/Co atomic ratio," *J. Alloys Compd.*, vol. 704, pp. 289–295, 2017.

[24] Q. Liu *et al.*, "Insights into size-dominant magnetic microwave absorption properties of CoNi microflowers via off-axis electron holography," *ACS Appl. Mater. Interfaces*, vol. 7, no. 7, pp. 4233–4240, 2015.

[25] X. Zheng *et al.*, "Amorphous FexB100− x nanostructures: Facile synthesis, magnetic properties and their applications as enhanced microwave absorbers at S-and C-bands," *Adv. Powder Technol.*, vol. 27, no. 2, pp. 704–710, 2016.

[26] Z. Liu, K. Suenaga, P. J. Harris, and S. Iijima, "Open and closed edges of graphene layers," *Phys. Rev. Lett.*, vol. 102, no. 1, p. 015501, 2009.

[27] O. V. Yazyev and M. Katsnelson, "Magnetic correlations at graphene edges: basis for novel spintronics devices," *Phys. Rev. Lett.*, vol. 100, no. 4, p. 047209, 2008.

[28] S. Wang *et al.*, "Giant edge state splitting at atomically precise graphene zigzag edges," *Nat. Commun.*, vol. 7, no. 1, p. 11507, 2016.

[29] Q. Sun *et al.*, "Coupled spin states in armchair graphene nanoribbons with asymmetric zigzag edge extensions," *Nano Lett.*, vol. 20, no. 9, pp. 6429–6436, 2020.

[30] D. A. Abanin, P. A. Lee, and L. S. Levitov, "Spin-filtered edge states and quantum Hall effect in graphene," *Phys. Rev. Lett.*, vol. 96, no. 17, p. 176803, 2006.

[31] Y. Plotnik *et al.*, "Observation of unconventional edge states in 'photonic graphene,'" *Nat. Mater.*, vol. 13, no. 1, pp. 57–62, 2014.

[32] J. Fernández-Rossier and J. J. Palacios, "Magnetism in graphene nanoislands," *Phys. Rev. Lett.*, vol. 99, no. 17, p. 177204, 2007.

[33] H. R. Matte, K. Subrahmanyam, and C. Rao, "Novel magnetic properties of graphene: presence of both ferromagnetic and antiferromagnetic features and other aspects," *J. Phys. Chem. C*, vol. 113, no. 23, pp. 9982–9985, 2009.

[34] T. Enoki and Y. Kobayashi, "Magnetic nanographite: an approach to molecular magnetism," *J. Mater. Chem.*, vol. 15, no. 37, pp. 3999–4002, 2005.

[35] C. Rao, H. R. Matte, K. Subrahmanyam, and U. Maitra, "Unusual magnetic properties of graphene and related materials," *Chem. Sci.*, vol. 3, no. 1, pp. 45–52, 2012.

[36] J. Jung, F. Zhang, and A. H. MacDonald, "Lattice theory of pseudospin ferromagnetism in bilayer graphene: Competing interaction-induced quantum Hall states," *Phys. Rev. B—Condensed Matter Mater. Phys.*, vol. 83, no. 11, p. 115408, 2011.

[37] K. Kusakabe and M. Maruyama, "Magnetic nanographite," *Phys. Rev. B*, vol. 67, no. 9, p. 092406, 2003.

[38] T. Enoki, Y. Kobayashi, and K.-I. Fukui, "Electronic structures of graphene edges and nanographene," *Int. Rev. Phys. Chem.*, vol. 26, no. 4, pp. 609–645, 2007.

[39] T. Enoki and K. Takai, "Unconventional electronic and magnetic functions of nanographene-based host–guest systems," *Dalton Trans.*, no. 29, pp. 3773–3781, 2008.

[40] X. Sun *et al.*, "Laminated magnetic graphene with enhanced electromagnetic wave absorption properties," *J. Mater. Chem. C*, vol. 1, no. 4, pp. 765–777, 2013.

[41] L. Quan, F. X. Qin, D. Estevez, H. Wang, and H. X. Peng, "Magnetic graphene for microwave absorbing application: Towards the lightest graphene-based absorber," *Carbon*, vol. 125, pp. 630–639, Dec. 2017, doi: 10.1016/j.carbon.2017.09.101.

[42] C. Wang *et al.*, "The electromagnetic property of chemically reduced graphene oxide and its application as microwave absorbing material," *Appl. Phys. Lett.*, vol. 98, no. 7, p. 072906, Feb. 2011, doi: 10.1063/1.3555436.

[43] M. M. M. Ahmed and T. Imae, "Electrochemical properties of a thermally expanded magnetic graphene composite with a conductive polymer," *Phys. Chem. Chem. Phys.*, vol. 18, no. 15, pp. 10400–10410, 2016, doi: 10.1039/C6CP00311G.

[44] S. Yu, F. Qin, and G. Wang, "Improving the dielectric properties of poly(vinylidene fluoride) composites by using poly(vinyl pyrrolidone)-encapsulated polyaniline nanorods," *J. Mater. Chem. C*, vol. 4, no. 7, pp. 1504–1510, 2016, doi: 10.1039/C5TC04026D.

[45] Q. Hao, X. Xia, W. Lei, W. Wang, and J. Qiu, "Facile synthesis of sandwich-like polyaniline/boron-doped graphene nano hybrid for supercapacitors," *Carbon*, vol. 81, pp. 552–563, Jan. 2015, doi: 10.1016/j.carbon.2014.09.090.

[46] Q. Yao, J. Xie, J. Liu, H. Kang, and Y. Liu, "Adsorption of lead ions using a modified lignin hydrogel," *J. Polym. Res.*, vol. 21, June 2014, doi: 10.1007/s10965-014-0465-9.

[47] F. Hossein-Babaei and E. Chegini, "The complex permittivity of PEDOT:PSS," *J. Chem. Phys.*, vol. 158, no. 19, p. 194904, May 2023, doi: 10.1063/5.0142523.

[48] D. Hamann, "Erratum: Optimized norm-conserving Vanderbilt pseudopotentials [Phys. Rev. B 88, 085117 (2013)]," *Phys. Rev. B*, vol. 95, June 2017, doi: 10.1103/PhysRevB.95.239906.
[49] H. Asadi and M. Vaezzadeh, "Computational designing ultra-sensitive nano-composite based on boron doped and CuO decorated graphene to adsorb H2S and CO gaseous molecules," *Mater. Res. Express*, vol. 4, June 2017, doi: 10.1088/2053-1591/aa7c33.
[50] C. Cao, M. Wu, J. Jiang, and H.-P. Cheng, "Transition metal adatom and dimer adsorbed on graphene: Induced magnetization and electronic structures," *Phys Rev B*, vol. 81, May 2010, doi: 10.1103/PhysRevB.81.205424.
[51] P. Mohn, "Magnetism in the Solid State: An Introduction," *Magn. Solid State Introd. Peter Mohn 2006 XI 229 P 72 Illus 1st Ed 2003 Corr 2nd Print. ISBN 3-540-29384-1 Berl. Springer 2006*, vol. 134, Jan. 2006.
[52] G. L. Krasko, "Structural properties of BCC and FCC iron: LMTO-ASA-Stoner calculations," *Solid State Commun.*, vol. 70, no. 12, pp. 1099–1103, June 1989, doi: 10.1016/0038-1098(89)90742-4.
[53] Y. Zhai, D. Zhu, W. Zhou, D. Min, and F. Luo, "Enhanced impedance matching and microwave absorption properties of the MAMs by using ball-milled flaky carbonyl iron-BaFe12O19 as compound absorbent," *J. Magn. Magn. Mater.*, vol. 467, pp. 82–88, Dec. 2018, doi: 10.1016/j.jmmm.2018.07.031.
[54] L. Wang *et al.*, "Orientation growth modulated magnetic-carbon microspheres toward broadband electromagnetic wave absorption," *Carbon*, vol. 172, pp. 516–528, Feb. 2021, doi: 10.1016/j.carbon.2020.09.050.